Background-Oriented Schlieren for the Detection of Thermoacoustic Oscillations in Flames

Sami Tasmany[1*], Daniel Kaiser[1], Jakob Woisetschläger[1*];
Johannes Gürtler[2], Robert Kuschmierz[2], Jürgen Czarske[2]

1: Institute for Thermal Turbomachinery and Machine Dynamics, Graz University of Technology, 8010 Graz, Austria
2: Laboratory of Measurement and Sensor System Technique, Faculty of Electrical and Computer Engineering, Technische Universität Dresden, Helmholtzstr. 18, 01062 Dresden, Germany

* Correspondenting author: sami.tasmany@tugraz.at

Keywords: Thermoacoustic Oscillations, Background-Oriented Schlieren, Laser interferometry, Chemiluminescence, Digital Fringe Analysis

ABSTRACT

Thermoacoustic oscillations are well known to combustion engineers. They are not only a cause of concern, but also give hope to be able to operate aircraft engines with hydrogen, due to flame stabilization and significant reduction of NOx emissions when thermoacoustically excited. The aim of this work is to investigate the potential of using a heterodyne background-oriented schlieren (HBOS) technique to detect thermoacoustic oscillations in the density field of an acoustically excited flame. It also seeks to address the issue of accuracy due to the small amplitude of thermoacoustic oscillations compared to turbulent density fluctuations in a flame. The experiment uses an unconfined swirl-stabilized methane flame and investigates thermoacoustic oscillations at about 3.4 kW power at ambient conditions excited by a siren at 225 Hz. The HBOS technique recently presented by the authors uses a carrier fringe system in background-oriented schlieren recordings, with subsequent analysis using evaluation techniques known from holographic interferometry. These fast algorithms reduce turbulence noise by phase averaging a large number of images. To derive local data from the line-of-sight projections, an inverse Abel transform is applied. Laser interferometric vibrometry is used to calibrate to the observed oscillations. A comparison with data from chemiluminescence is also presented to better demonstrate the application of this efficient technique to the detection of heat release oscillations. Future tasks in this project will deal with full-scale test benches and machine learning tools to address the limited observations in them.

1. Introduction

Low frequency pressure oscillations in the range of 50 - 120 Hz (rumble, hum) are typical of combustion processes. They occur especially at the limit of stable combustion, e.g. in lean-burn aircraft engines. In this case, immediately after the nozzle, there is a vortexing of the flow with alternating zones of compression and expansion of the gas. Fuel droplets vaporize faster in areas of accelerated expansion and more slowly in areas of compression. This results in oscillations in

heat release (hot and cold spots), turbulence, and in the mixture of reactants and combustion products. The resulting waves are entropy waves. If these oscillations are properly phased, the oscillation can be amplified as it is reflected back to the burner as a pressure wave from the first stage nozzle. With the exception of a few special applications, combustion oscillations are an undesirable phenomenon that can lead to loss of efficiency, component fatigue, and unwanted noise (Steinberg and Driscoll 2009; Dowling and Mahmoudi 2015). In lean premixed hydrogen combustion in the kW range, the combustion might benefit from forced thermoacoustic oscillations (Paulitsch et al. 2023). By these oscillations, Paulitsch et al. (2023) force the flame to stabilize further away from the injection, thereby increasing the mixing rate, energy density, and combustion efficiency, leading to reductions in NO_x emissions. The hydrogen flame appears to be more robust to lean blowout when thermoacoustically excited, while at the same time improving combustion performance.

In a previously submitted manuscript (Tasmany et al. 2024), we introduced a heterodyne background-oriented schlieren (HBOS) technique. This HBOS technique heterodynes a carrier fringe system in background-oriented schlieren recordings, with subsequent analysis using evaluation techniques known from holographic interferometry. The fast algorithms inherent in heterodyne techniques allow a large number of recordings to be evaluated, overcoming the problem of long evaluation time due to high turbulence, which requires a large number of recordings for each phase step of the oscillation. Image distortion can be handled by background subtraction, and the field of view (FOV) is no longer limited by large, high-quality telecentric lenses. In addition to refractive index or density oscillations, HBOS provides visualization of turbulence oscillations in the combustion zone, and also provides a tool to test for thermoacoustic oscillations. The test object in this research is an unconfined swirl-stabilized methane flame operated at approximately 3.4 kW power and ambient conditions excited by a siren at 225 Hz.

In this Proceedings of the 21st International Symposium on the Application of Laser and Imaging Techniques to Fluid Mechanics we will focus on the procedure and the possibilities offered by HBOS for phase stepped detection of thermoacoustic oscillations.

2. Materials

A schematic of the setup is shown in Figure 1. For these initial tests, we used an unconfined swirl-stabilized flame operated at approximately 3.4 kW power. A methane mass flow of 0.074 g/s and an air mass flow of 1.320 g/s were premixed and fed to the burner. A tangential to axial gas flow ratio of 0.803 resulted in an equivalence ratio of 0.95 and a swirl number of 0.53. The operating conditions are the same as those published by Greiffenhagen et al. (2020). A siren (Giuliani et al.

2020) introduced pressure oscillations at 225 Hz in the axial supply line and provided the trigger signal for all measurements.

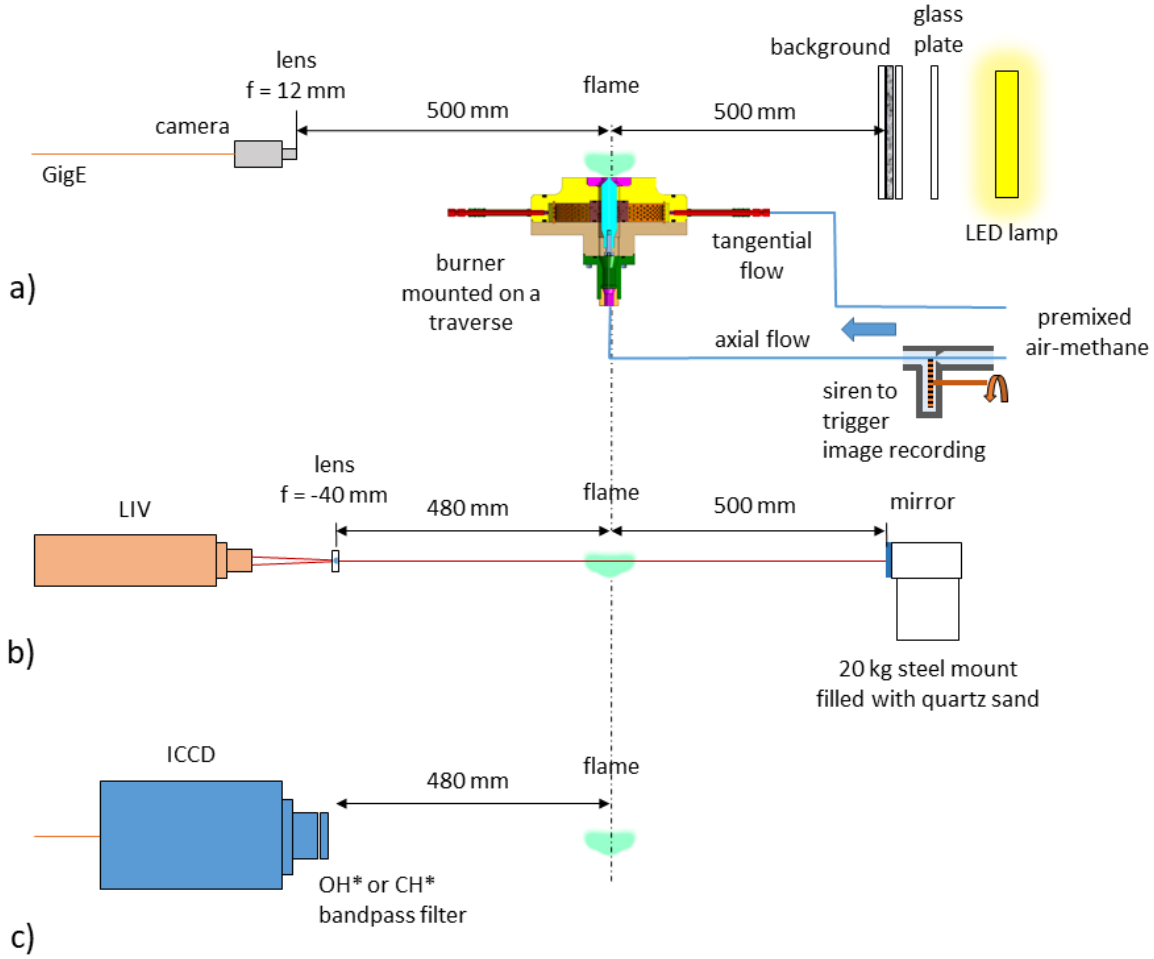

Figure 1 Section a) shows the experimental setup for the Heterodyne Background Oriented Schlieren (HBOS) method to detect refractive index and density variations in a swirl-stabilized lean air-methane unconfined flame of about 3.4 kW power. The background pattern is glued to a glass plate, with a second glass plate behind to shield the heat radiation emitted from the battery powered 50 W LED lamps. The siren trigger signal is used for phase-averaging. Section b) presents the experimental setup for the laser interferometry vibrometry (LIV) recordings used to calibrate the HBOS measurements. Section c) presents the details of the chemiluminescence measurements using an intensified CCD (ICCD) and bandpass filters to record the OH* or CH* emission from the flame.

For HBOS, a GigE monochromatic camera (CMOS sensor, Sony IMX273) with a 12 mm focal length lens (acA1440-73gm and lens C23-1224-5M-P, Basler AG, Ahrensburg, Germany) and a resolution of 1440 × 1080 px was placed at a distance of 500 mm from the burner, facing the flame. At this magnification, one pixel corresponds to a length of approximately 0.1 mm in object space. The camera was set to gain 110 at F-number 5.6 and an exposure time of 1/2000 s. A fringe background pattern was printed on a diffusing paper (RTL49 A3, Altiel Limited, United Kingdom) and then glued to the side of the plate facing the flame, with a second glass plate clamped on top to avoid unwanted movement of the pattern. Five battery-powered LED lights of 50 W

(800 - 4500 lm Li-Ion 5200 mAh 14.8 V) were used to illuminate the background pattern. To shield the fringe pattern plate from the heat radiated by the lamps, a 6 mm thick glass plate was placed between the lamps and the background pattern. The background pattern was a 1 mm modified grid pattern obtained by reducing the spectral diagonal components of the image signal (see Tasmany et al. 2024 and Figure 2A).

To calibrate the HBOS a OFV-503 sensor head (Polytech GmbH, Waldbronn, Germany) and an OFV-5000 vibrometer controller (Decoder VD-06, Polytech GmbH, Waldbronn, Germany) with a 20 kHz low-pass filter and a sensitivity of 2 mm s^{-1} V^{-1} were used. A lens with a focal length of - 40 mm was located 480 mm from the flame axis to obtain a collimated beam of approximately 1.5 mm in diameter. The use of laser interferometric vibrometry (LIV) to detect density oscillations in combustion is discussed in Greiffenhagen et al. (2019).

As a reference, OH* and CH* chemiluminescence were recorded with an intensified CCD (ICCD) camera (NanoStar, 1280 × 1024 pixels, photocathode radiation sensitivity 310 nm/430 nm = 65%, DaVis V7.2.2.456 software, LaVision, together with a UV lens, 105 mm, f/4.5, Nikon). A 310 nm and a 430 nm bandpass filter were used for OH* emission and CH* emission, respectively (310 ± 3 nm CWL, FWHM 10 ± 2 nm bandwidth, 18% transmission, and 430 ± 2 nm CWL, FWHM 10 ± 2 nm bandwidth, 98% transmission, both Edmund Optics). Background images were recorded and subtracted for all measurements.

3. Methods

In the schlieren method, the displacement Δx of a background pattern can be related to the deflection of light rays by gradients in refractive index n or density:

$$\Delta x = l \int \frac{1}{n} \frac{\partial n}{\partial x} \, dz \approx l \frac{\partial}{\partial x} n_{LOS} \tag{1}$$

With l the distance between background and flame, z the coordinate along the light ray, x the horizontal and y the vertical coordinate. The schlieren method is a line of sight (LOS) method. This means that all gradients along the path of the beam are summed. At ambient conditions the refractive index is so close to one that the displacement is assumed to be directly proportional to the refractive index gradients. In high pressure combustion the $(ln\ n)_{LOS}$ must be used instead of n_{LOS} in eq. 1. A detailed discussion of the BOS technique can be found in Raffel (2015).

Instead of a speckled pattern, other authors used parallel fringes or grid structures to detect the displacement Δx (Perciante and Ferrari 2000; Blanco et al. 2016 a, b; Vinnichenko et al. 2023). A well-known technique in holographic interferometry is to superimpose a carrier frequency on a signal, in this case the pattern displacement, and then to demodulate the signal (Osten 1991; Kreis 2005). Spatial heterodyning and subsequent filtering and demodulation allow the detection of

fractions of a fringe period (sub-fringe analysis). Based on Figure 2, we follow the evaluation as recently proposed by the authors (Tasmany et al. 2024).

The intensity distribution $i(x,y)$ in the fringe pattern is comprised of the background intensity $i_0(x,y)$, the fringe amplitude $a(x,y)$, the phase related to the heterodyned carrier fringe system $\varphi_c(x,y)$, and $\varphi_d(x,y)$, which is the phase related to the displacement of the carrier fringe system due to the beam deflections by the refractive index gradients:

$$i(x,y) = i_0(x,y) + a(x,y)\cos[\varphi_c(x,y) + \varphi_d(x,y)] \tag{2}$$

In this equation $\varphi_d(x,y)$ is in a linear relationship to Δx (in pixel) by

$$\frac{2\pi}{\lambda} = \frac{\varphi_d(x,y)}{\Delta x(x,y)} \tag{3}$$

λ is the period of the carrier fringes, here 8.6 px. The following discussion is for the base frequency and can be found in the textbooks on holographic interferometry by Osten (1991) and Kreis (2005). Figure 2A shows a single recording of the grid-like background together with the displacement of the background by the LOS gradients in the flame. The grid was modified along the diagonal structures to reduce the crosstalk between diffraction orders in the Fourier spectra. The next step is a two-dimensional Fourier transform of each of the 10,000 images recorded for time-averaged recordings and eight phase steps of oscillation at 225 Hz. The Fourier spectra were then averaged and the results are shown in Figure 2B. A bandpass filter was applied from 63 cycles per frame to 272 cycles along the abscissa with a height of ± 70 cycles per frame to detect the displacements in the x-direction, and from 49 cycles per frame to 205 cycles per frame along the ordinate with a width of ± 94 cycles per frame to detect the displacements in the y-direction. A window of similar size was used to record the noise level. The resulting phase uncertainty from the SNR was estimated to be ± 0.027 px for the horizontal displacement and ± 0.028 px for the vertical displacement, according to Rathjen (1995). For the background images with only the carrier fringes and without the flame, the values are ± 0.026 px and ± 0.027 px, respectively. All filter positions are shown in Figure 2B. After an inverse Fourier transform with the applied filters, a modulo-2π plot of the phase distribution in the image domain was derived. Using the Euler equation and back to the image domain, we can write

$$i(x,y) = i_0(x,y) + g(x,y) + g^*(x,y) \tag{4}$$

with

$$g(x,y) = \frac{1}{2}\, a(x,y) e^{+j\,[(\varphi_c(x,y) + \varphi_d(x,y)]} \tag{5}$$

and

$$\varphi_c(x,y) + \varphi_d(x,y) = arctan2\, \frac{Im[g(x,y)]}{Re[g(x,y)]} \tag{6}$$

$$a(x,y) = 2\sqrt{g(x,y)g^*(x,y)} \tag{7}$$

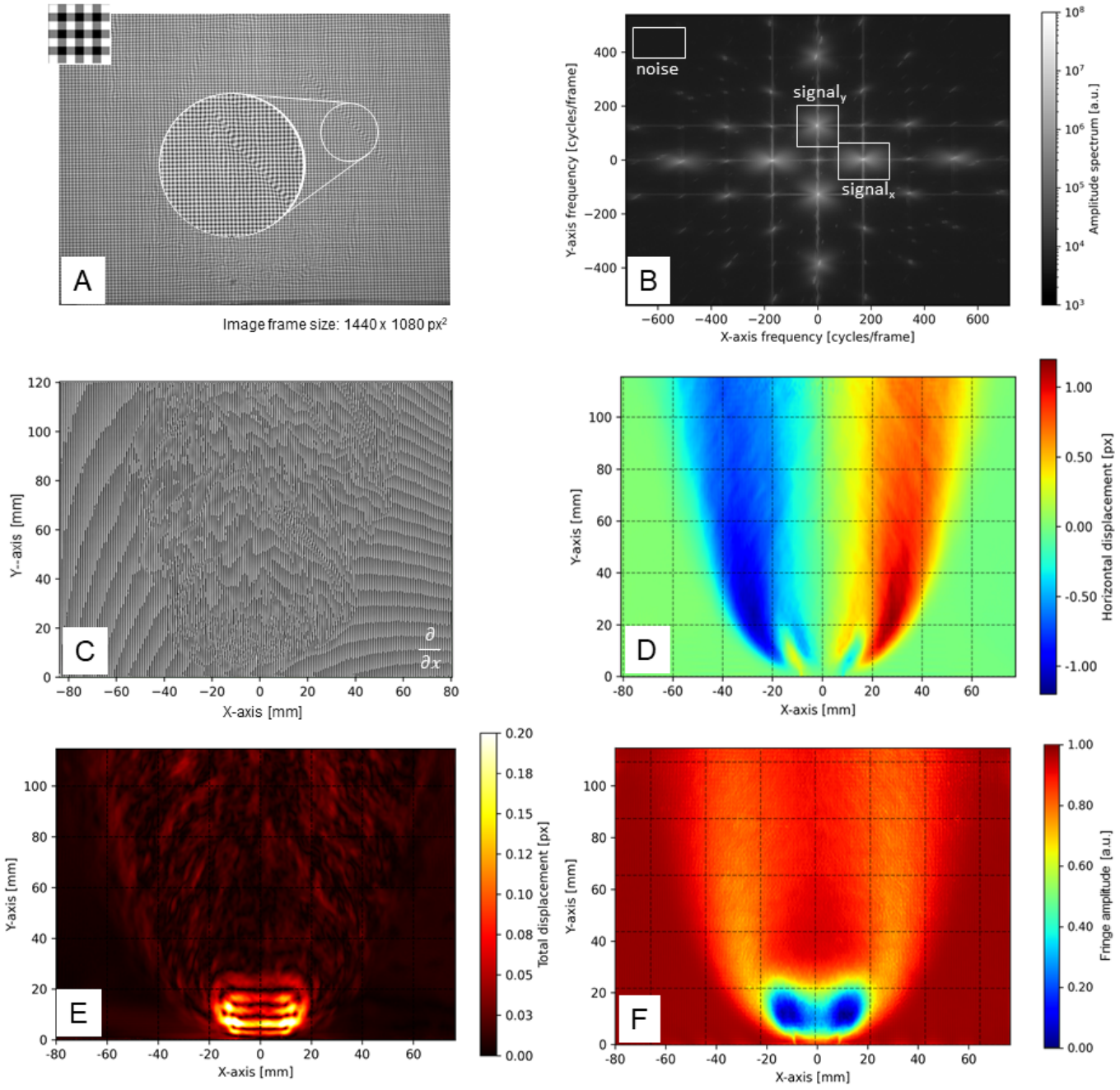

Figure 2 Section A shows the intensity distribution in a single frame, with a focus on the displacement of the background pattern by the flame. The background grid was modified along the diagonal structures to reduce the crosstalk between diffraction orders in the Fourier spectra. Section B plots the frequency spectrum averaged on 10,000 recordings together with the filters used to derive the displacements in x- and y- direction, as well as the SNR. Section C provides the modulo-2π phase distribution for a single recording. Section D shows the horizontal displacement after transformation of the phase distribution into the displacement according to equation 3, and after background subtraction. Finally, section E presents the oscillation for a single phase-step in terms of absolute

displacement. Section F illustrates the fringe modulation, a consequence of blurring and defocusing effects of strong gradients, mainly in high-frequency turbulence regions.

The Fourier transform and filtering were conducted by the dft module from the Python OpenCV library, while the unwrapping of the modulo-2π phase distribution was performed by the unwrap_phase module from the Python scikit-image library. The modulo-2π plot for the horizontal displacement is presented in Figure 2C for a single recording. In order to calculate the modulation phase $\varphi_d(x,y)$, 10,000 background images with the carrier fringes system only were evaluated with the same filters as previously described and subtracted from the total phase distribution as given in equation 6. The background subtraction process has the effect of compensating not only the carrier signal but also any local perturbations in the fringe system. Since Equation 3 relates the displacement to the phase via the period of the carrier fringe system, great care must be taken since the carrier fringe system may vary over the image due to perspective distortions. Here, the carrier frequency variations over the FOV were less than 0.5%, so no correction algorithm was applied. As a result of this procedure, the displacements in the x- and y-directions are derived from the phase distribution, with the displacement in the x-direction shown in Figure 2D. A spatial resolution of 3.5 px in the displacement fields results from the Nyquist-Shannon theorem and the image size (1440 × 1080 px), the filter width of 210 px in the x-direction and 157 px in the y-direction.

A total of nine displacement distributions were recorded, one as a time-averaged recording with 10,000 frames and no trigger, and eight phase-averaged recordings, again with 10,000 frames each, triggered by the siren. Phase-averaging means that each image is assigned to a phase of the 225 Hz oscillation. The recording time of all images was chosen to be less than the time between the equally spaced phase steps. Figure 2E shows the displacement field of the oscillation as a result of this procedure. The magnitude of the displacement is plotted as the vectorial difference between the phase-averaged and time-averaged fields for one phase step. The techniques of heterodyne holographic interferometry also provide the modulation of the fringe pattern, as shown in Figure 2F. This modulation is a consequence of blurring and defocusing effects of strong gradients and high-frequency turbulence regions. In the combustion zone, these plots are similar in shape to the OH* emission plots shown in Greiffenhagen et al. (2020), which mark the location of heat release. It is important to note that high-frequency and small-scale turbulence is underestimated in LOS fringe amplitude blurring due to the LOS averaging (Mayrhofer and Woisetschläger 2001). Therefore, for the high-turbulence and combustion regions in the flame, the modulation of fringe amplitude is a qualitative measure only.

The displacement in x- direction (as shown in Figure 2 D) can be used to calculate the local distribution of refractive index by the inverse Abel transform

$$n(r) = -\frac{1}{\pi}\int \frac{dn_{LOS}}{dx}\frac{1}{\sqrt{x^2-r^2}}\,dx \tag{8}$$

In this work, we directly used the derivative of the refractive index as given by Equation 1 to solve this equation as suggested by Pretzler et al. (1993). The cylindrical symmetry requirement of this flame has been verified by Greiffenhagen et al. (2020). The Python module abel.direct of the PyAbel library was used to compute the tomographic sections.

In order do calculate the local density fields of oscillation for eight phase steps, the local time-averaged distribution and the eight phase-averaged data sets were first subtracted and then calibrated by the LOS data from the LIV to obtain the local oscillations in refractive index. The refractive index local oscillations were then transformed into density oscillations by the Gladstone Dale relation

$$n - 1 = G\,\rho \qquad , \tag{9}$$

with the Gladstone Dale number G and ρ the density. According to Gardiner et al. (1981) and using the gaseq software (Morely 2005) to obtain molar concentrations for reactants and products in the combustion zone, the Gladstone-Dale number was derived. For lean combustion of hydrocarbons, the difference in the Gladstone-Dale number between products and reactants is less than 0.5%, indicating that a single average value can be applied. In this case, an average value of 2.45×10^{-5} m^3kg^{-1} was used.

To compare the results from the fringe amplitude, time-averaged intensities, and phase-averaged intensities, we recorded the OH* and CH* radicals' emission. Figure 3 presents two time steps for the OH* emission. During the evaluation of the emission shown in Figure 3, a background subtraction was performed.

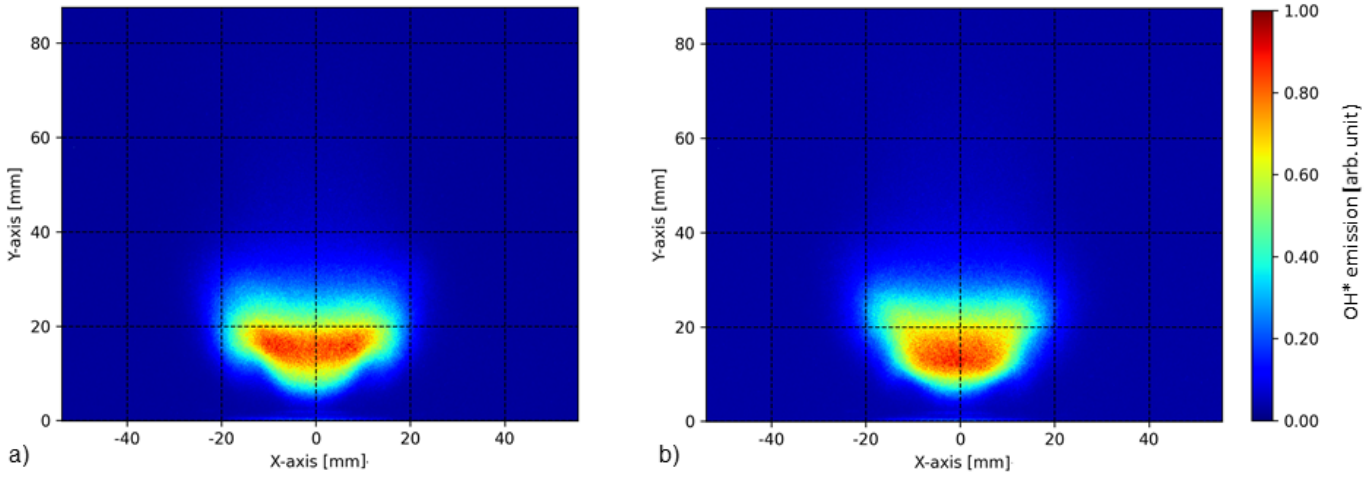

Figure 3 Intensity emitted by the OH* radicals during two phase steps during the 225 Hz thermoacoustic oscillation.

3. Results and Discussion

In the given configuration with a distance of 0.5 m between the background and the flame (about 3.4 kW power), the displacement of the background pattern is in the range of one pixel. The sensitivity can be increased by increasing the distance between the background pattern and the flame. Due to the small aperture of the camera used (F-number 8), the chosen distances allowed a sharp image of the background pattern even in the presence of a strong gradient. Thus, the blurring of the image was mainly due to turbulence on timescales faster than the exposure time.

Figure 4a shows an oscillation cycle of 225 Hz divided into 8 time steps. Only the gradient in the x-direction is plotted. Since tomography calculates the local data in cross sections, the gradient in the reconstruction plane would be sufficient to obtain local values for refractive index or density (cf. Equation 8). To cover 180° of observation in one plane is possible only under laboratory conditions, but not for real sized burners. In these, multidirectional observation includes horizontal and vertical directions. In the near future, we also plan to use a deep learning algorithm to better compensate for missing directions. To enable three-dimensional observation, we decided to use a grid as a background pattern and perform a 2-dimensional Fourier transform to obtain the displacement as a vector.

In Figure 4b, the displacements (gradients) are plotted for the oscillation only. For this purpose, the vectorial difference of the two components of the gradient has to be plotted, which is obtained from the difference between the single time-averaged and the eight phase-averaged data. To minimize the turbulent noise in the downstream flow, 10,000 frames had to be averaged. Figure 4b is for discussion only, since for tomographic reconstruction the nine full-fields have to be tomographically reconstructed and then subtracted to obtain information about the local refractive index or density oscillation.

Figure 4 shows only the magnitude of the gradients. To better discuss what is happening in the LOS data, color coding was applied, similar to the color schlieren visualization proposed by Settles (1970). In Figure 5, green and red indicate the horizontal directions of the gradients, and blue and yellow indicate the vertical components. From this color representation it can be seen that in this first time step at position (-12/+8 mm) there is a cold spot in the LOS data, while at position (-17/+15 mm) there is a hot spot, as indicated by the circles in Figure 5. Comparing these two positions, the color of the horizontal gradients changes at these positions.

Figure 6 shows the magnitude of the difference between time-averaged and phase-averaged fringe amplitude data. This modulation is mainly a consequence of blurring in high frequency turbulence regions which mark the location of heat release (hot spots), and is similar in shape to

the oscillations in the OH* and CH* emissions seen in Figure 7. Due to the fact that small

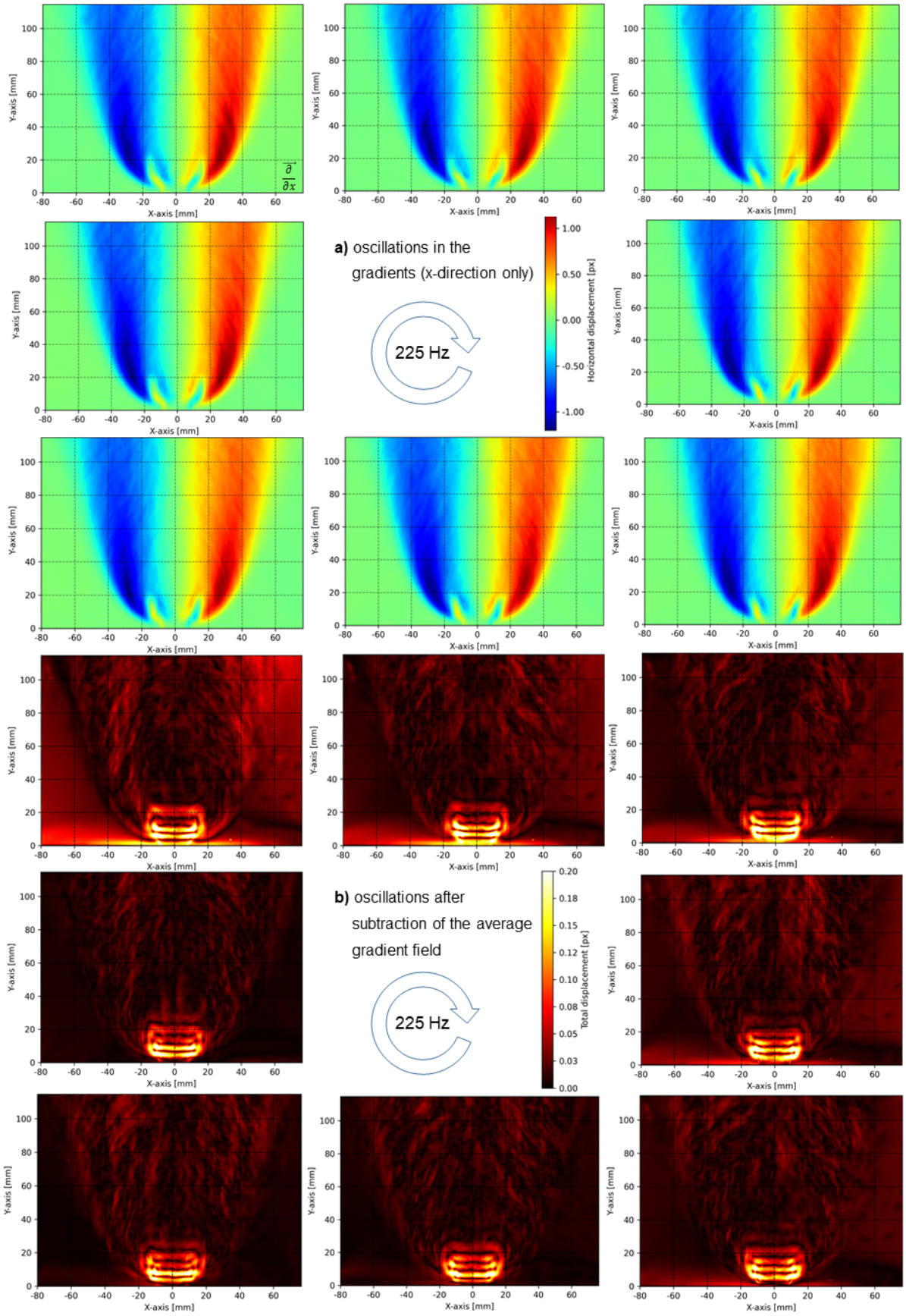

Figure 4 a) shows the displacement (gradient) in x-direction for eight phase steps, while b) shows the magnitude of the displacement calculated from the vectorial difference between time-averaged and phase-averaged LOS data.

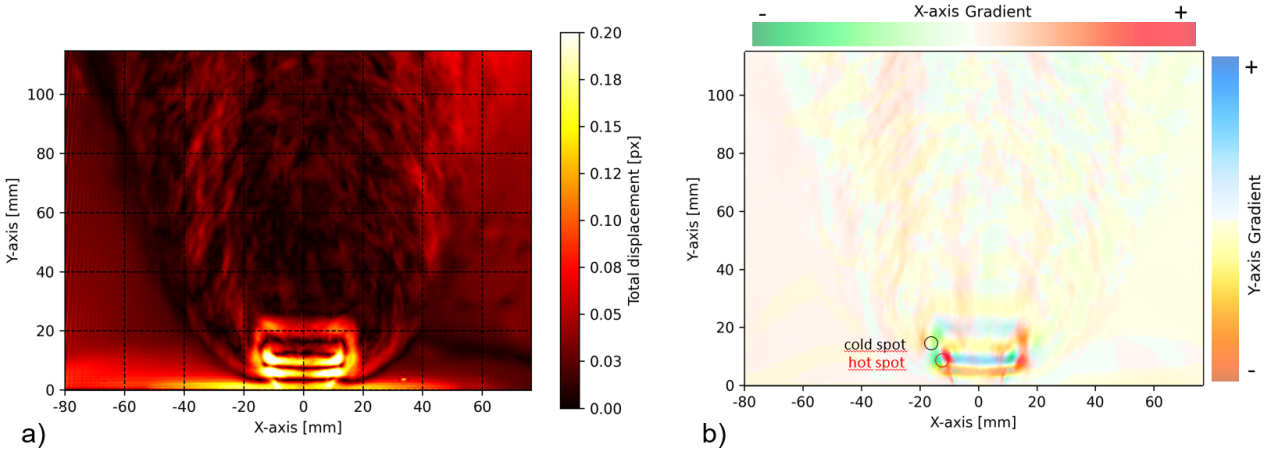

Figure 5 a) shows the magnitude of the displacement (gradients) calculated from the vectorial difference between time-averaged and phase-averaged LOS data, while b) color-codes the displacements (gradients).

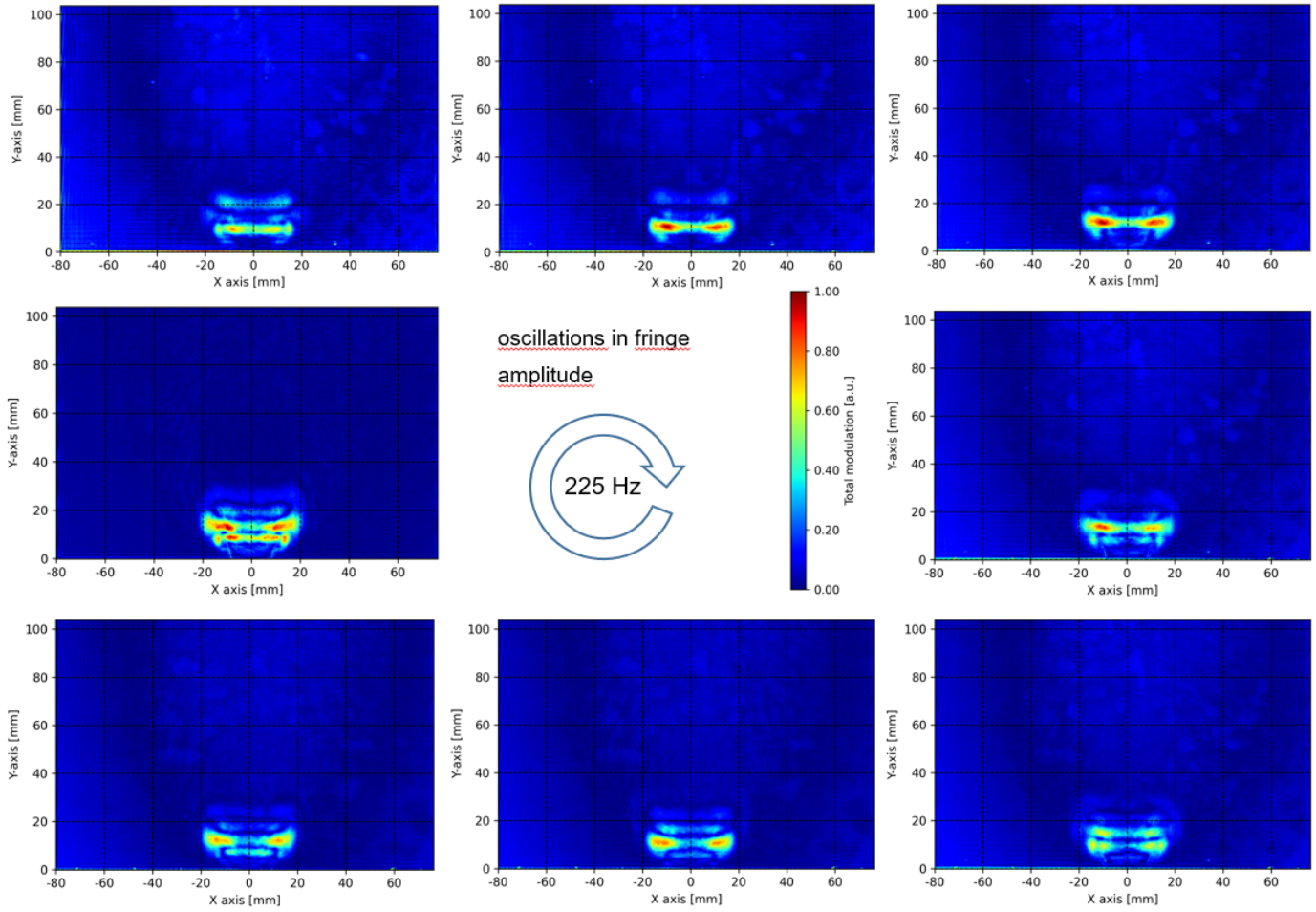

Figure 6 Oscillations in fringe amplitude. Plotted is the difference between time-averaged and phase-averaged data for the fringe amplitude. This modulation is mainly a consequence of blurring in high-frequency turbulence regions that mark the location of heat release (hot spots), and is similar in shape to the OH* emission oscillations seen in

Figure 7b. Due to the LOS nature of these plots and the small size of the turbulent eddies the modulation of fringe amplitude is a qualitative measure only (see Mayrhofer and Woisetschläger 2001). All data are LOS data.

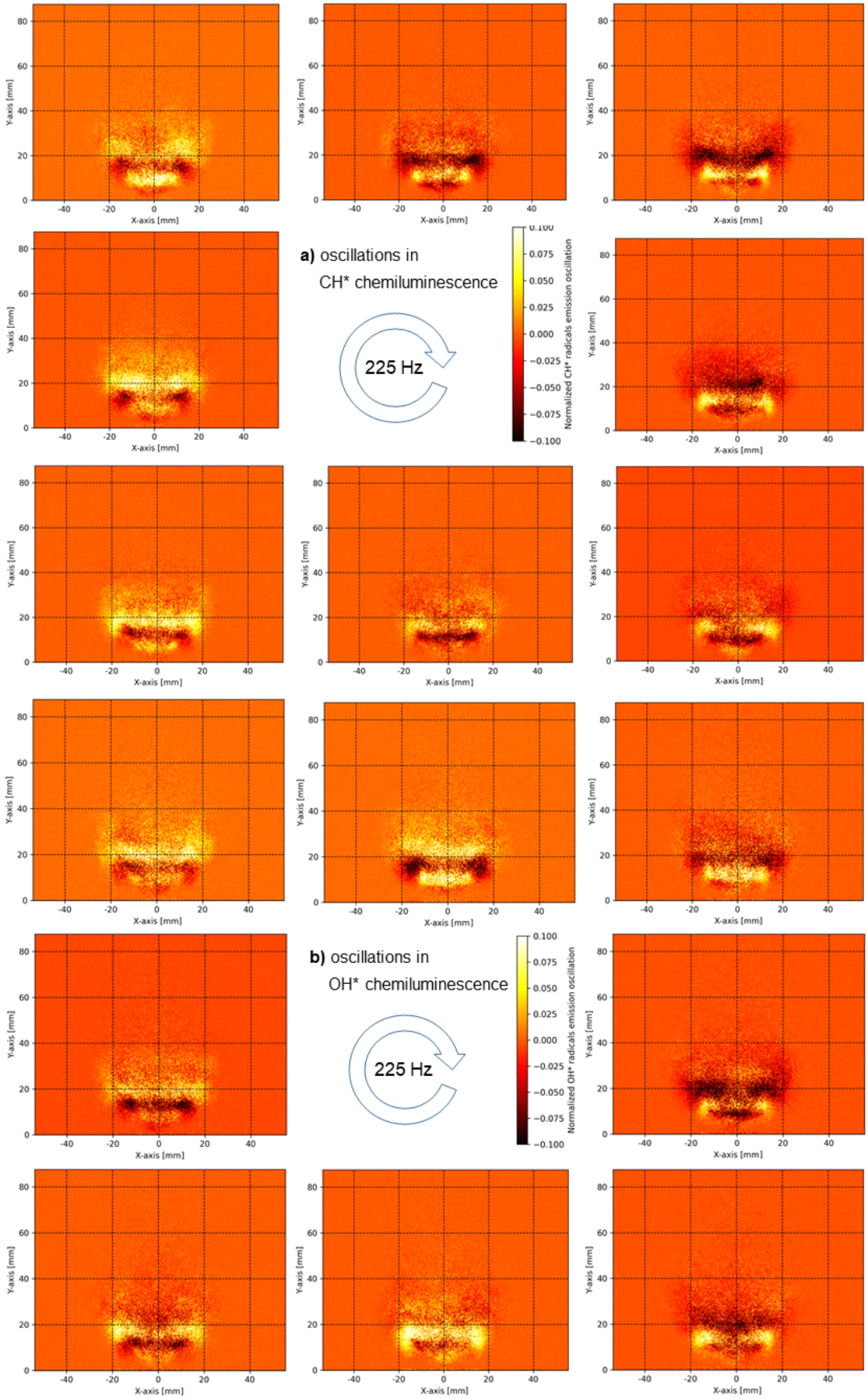

Figure 7 Normalized oscillations in CH* (a) and OH* (b) emission calculated from the difference between time-averaged and phase-averaged data. All data are LOS data.

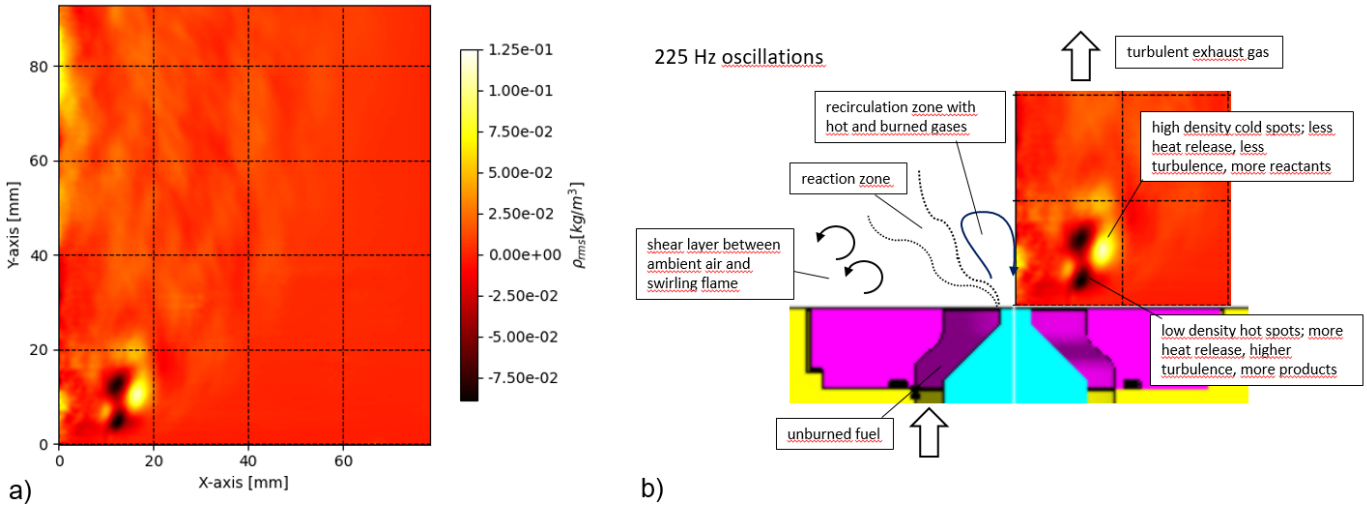

Figure 8 a) Local density oscillations at 225 Hz and b) discussion of the flow field (cmp Lauer 2011).

and oscillating turbulent structures along the beam path may average out, these fringe amplitude modulation plots are only qualitative in identifying oscillations in turbulence by the combustion (cf. Mayrhofer and Woisetschläger 2001). On the other hand, they serve to mark the turbulent regions and can be used to check the significance of the density oscillations detected by HBOS.

The OH* and CH* plots in Figure 7 are calculated from the difference between one time-averaged and eight phase-shifted recordings. Each recording is a (phase) average of more than 3000 frames. The OH* and CH* emissions serve as an indication of heat release and as a marker for the flame front. The ratio of OH*/CH* radical emission gives the equivalence ratio. A detailed discussion of chemiluminescence can be found in Lauer (2011). While in lean methane combustion the Gladstone Dale numbers of products and reactants are close, in other fuels this ratio can provide a correction for the local Gladstone Dale number. In the unconfined flame discussed here, the region with the largest variation in Gladstone Dale number is the outer flame region, where cold, fresh air can mix with the premixed fuel. This difference in Gladstone Dale number between air and fuel (products and reactants at an equivalence ratio of 0.95) can lead to uncertainties of up to 9% (see Greiffenhagen et al. 2020).

The final step requires a tomographic reconstruction of the local distribution of the refractive index. Here, the horizontal gradients were used to solve the inverse Abel transform (Equation 8) for all nine recordings (one time-averaged and eight phase-averaged recordings). The oscillation amplitude was calculated from the difference between the time-averaged and phase-averaged data sets. LOS oscillation data were then recalculated from the tomographic cross sections and compared to the LOS oscillation amplitudes recorded by the LIV system in a single plane 10 mm above the nozzle of the flame. In this way, the LIV recordings served as a calibration for the

refractive index oscillations. Finally, density oscillations were calculated from these local refractive index data and are plotted in Figure 8a for a half plane in the flame region. While LIV provides local density oscillations only, HBOS can provide local oscillations and the time-averaged local density distribution. Both fields are needed to calculate the heat release oscillations (Greiffenhagen et al. 2019, 2020).

Figure 8b discusses the propagation of hot and cold spots in the curled flame front, together with the shear layer between ambient air and unburned fuel in this open unconfined flame. From the shedding period of the hot and cold spots (about 0.2 m) and the frequency of 225 Hz, a velocity of the entropy waves of about 10 m/s is estimated. A number that compares well with previous results in Greiffenhagen et al. (2020). There the bulk velocity was estimated to be about 8 m/s. Based on the time-averaged data, a cylindrical symmetry is currently assumed, which is unlikely for the oscillating entropy waves due to the swirling nature of these flames. Therefore, a multidirectional observation is planned in this project.

4. Conclusions and Outlook

Thermoacoustic oscillations can be detected by HBOS. HBOS uses a carrier fringe system as a background pattern with subsequent analysis by evaluation techniques known from holographic interferometry. This heterodyne technique, based on Fourier transforms, allows the evaluation of large data sets needed to reduce noise from turbulence in the flow. Local density oscillations in combustion can be calculated by subsequent analysis directly on the LOS gradients. The modulation of the fringe amplitude marks the regions of high turbulence associated with heat release in the combustion zone (hot spots). This feature of HBOS allows to visualize heat release oscillations in addition to density oscillations, but is used for visualization only. HBOS also provides local density oscillations and the local time-averaged density field, both of which are needed to calculate local heat release oscillations in the combustion region. Future work on this project will focus on multidirectional observation with up to 18 cameras and the application of deep learning algorithms for limited angles of observation.

Acknowledgments

This research is the result of Austrian-German joint research project, funded by the Austrian Science Fund FWF within grant FWF-I5392-N and the Deutsche Forschungsgemeinschaft DFG within grant CZ 55/50-1. This project is a Lead-Agency D-A-CH project in cooperation between Graz University of Technology, Austria and Technische Universität Dresden, Germany, named "Four-dimensional measurement of thermoacoustic oscillations”.

Repository

The Python routines and some data utilized in this project are available for download from the TU Graz repository (Tasmany and Woisetschläger 2024).

References

Blanco A, Barrientos B, Mares C (2016 a) Performance comparison of backgroundoriented schlieren and fringe deflection in temperature measurement: part I. Numerical evaluation. Optical Engineering 55(5):054102. https://doi.org/10.1117/1.OE.55.5.054102

Blanco A, Barrientos B, Mares C (2016 b) Performance comparison of backgroundoriented schlieren and fringe deflection in temperature measurement, part 2: experimental evaluation. Optical Engineering 55(6):064104. https://doi.org/10.1117/1.OE.55.6.064104

Dowling, A.P., Mahmoudi, Y. (2015) Combustion noise. Proceedings of the Combustion Institute 35(1):65–100. https://doi.org/10.1016/j.proci.2014.08.016

Gardiner, W., Hidaka, Y., Tanzawa, T. (1981) Refractivity of combustion gases. Combustion and Flame 40:213–219. https://doi.org/https://doi.org/10.1016/0010-2180(81)90124-3

Giuliani, F., Stütz, M., Paulitsch, N., Andracher, L. (2020) Forcing pulsations by means of a siren for gas turbine applications. Int. J. Turbomach. Propuls. Power 5(2):9. https://doi.org/10.3390/ijtpp5020009

Greiffenhagen, F., Peterleithner, J., Woisetschläger, J., Fischer, A., Gürtler, J., Czarske, J. (2019) Discussion of laser interferometric vibrometry for the determination of heat release fluctuations in an unconfined swirl-stabilized flame. Combustion and Flame 201:315–327. https://doi.org/10.1016/j.combustflame.2018.12.019

Greiffenhagen, F., Woisetschläger, J., Gürtler, J., Czarske, J. (2020) Quantitative measurement of density fluctuations with a full-field laser interferometric vibrometer. Exp Fluids 61:9. https://doi.org/10.1007/s00348-019-2842-y

Kreis, T. (2004) Handbook of holographic interferometry. In: Wiley-VCH Verlag GmbH & Co. KGaA, Weinheim. https://doi.org/10.1002/3527604154

Lauer, M. R. W. (2011) Determination of the Heat release distribution turbulent flames by chemiluminescence imaging. Doctoral Thesis, Technische Universität München. https://mediatum.ub.tum.de/doc/1071121/1071121.pdf (access 2024-05-27)

Mayrhofer, N., Woisetschläger, J. (2001) Frequency analysis of turbulent compressible flows by laser vibrometry. Experiments in Fluids 31:153–161. https://doi.org/10.1007/s003480000268

Morley, Ch. (2005) A Chemical Equilibrium Program for Windows, V 079b, http://www.gaseq.co.uk/ (access 2024-05-27)

Osten, W. (1991) Digitale Verarbeitung von Interferenzbildern, Akademie Verlag Berlin, ISBN 3-05-501294-1

Paulitsch, N., Giuliani, F., Hofer, A., Hofer, J., Andracher, L. (2023) Progress on the Complete and Low-NOx Combustion of Eco-Fuels Using a Thermo-Acoustically-Driven, Hydrogen-Powered Pilot Stage. Proceedings of the ASME Turbo Expo 2023: Turbomachinery Technical Conference and Exposition. Volume 2: Ceramics and Ceramic Composites; Coal, Biomass, Hydrogen, and Alternative Fuels. Boston, Massachusetts, USA. June 26–30, 2023. V002T03A018. ASME. https://doi.org/10.1115/GT2023-102987

Perciante CD, Ferrari JA (2000) Visualization of two-dimensional phase gradients by subtraction of a reference periodic pattern. Appl. Opt. 39(13):2081–2083. https://doi.org/10.1364/AO.39.002081

Pretzler, G., Jäger, H., Neger, T. (1993) High-accuracy differential interferometry for the investigation of phase objects. Meas. Sci. Technol. 4:649. https://doi.org/10.1088/0957-0233/4/6/003

Raffel, M., (2015) Background-oriented schlieren (BOS) techniques. Exp Fluids 56:60. https://doi.org/10.1007/s00348-015-1927-5

Rathjen C (1995) Statistical Properties of phase-shift algorithms, J. Opt. Soc. Am. A 12:1997-2008, https://doi.org/10.1364/JOSAA.12.001997

Settles, G. (1979) A direction-indicating color schlieren system. AIAA Journal. 8:2282–2284 https://doi.org/10.2514/3.6106

Steinberg, A.M., Driscoll, J.F. (2009) Straining and wrinkling processes training and wrinkling processes during turbulence–premixed flame interaction measured using temporally-resolved diagnostics. Combustion and Flame 156, 2285–230 http://dx.doi.org/10.1016/j.combustflame.2009.06.024

Tasmany, S., Kaiser, D., Woisetschläger, J., Gürtler, J., Kuschmierz, R., Czarske, J. (2024) Heterodyne background - oriented schlieren for the measurement of thermoacoustic oscillations in flames. submitted to Exp Fluids

Tasmany S, Woisetschläger J (2024). Heterodyne Background-Oriented Schlieren for the Measurement of Thermoacoustic Oscillations in Flames [Data set]. Graz University of Technology. https://doi.org/10.3217/7k9f0-7wb03

Vinnichenko N, Pushtaev AV, Plaksina YY, Uvarov AV (2023) Performance of background oriented schlieren with different background patterns and image processing techniques. Experimental Thermal and Fluid Science. 147:110934. https://doi.org/10.1016/j.expthermflusci.2023.110934